Ferrimagnetic Nanogranular Co_3O_4 through Solvothermal Decomposition of Colloidally Dispersed Monolayers of α-Cobalt Hydroxide

C. Nethravathi,[†] Sonia Sen,[†] N. Ravishankar,[‡] Michael Rajamathi,*[,†] Clemens Pietzonka,[§] and Bernd Harbrecht*[,§]

Department of Chemistry, St. Joseph's College, 36, Lalbagh Road, Bangalore 560 027, India, Materials Research Center, Indian Institute of Science, Bangalore 560 012, India, and Department of Chemistry and Center of Materials Science, Philipps University, D-35032 Marburg, Germany

Received: February 10, 2005; In Final Form: April 8, 2005

Co_3O_4 nanoparticles of 35 nm with a cauliflower-like morphology were obtained when a monolayer colloidal dispersion of dodecyl sulfate intercalated α-cobalt hydroxide in butanol was subjected to solvothermal hydrolytic decomposition. The nanogranular particles exhibit weakly ferromagnetic properties in contrast with both bulk and dispersed nanoparticulate Co_3O_4.

Introduction

Magnetic nanoparticles are of great importance as they are potent materials for applications in varied fields. The size reduction of a magnetic material leads to novel properties such as superparamagnetism;[1] that is, with decreasing particle size the magnetic anisotropy energy per particle responsible for holding the magnetic moment along certain directions becomes comparable to thermal energy. The thermal energy will then induce random flipping of the magnetic moment with time and the magnetic particles will lose their magnetic order. Another property that arises from size reduction is spin canting,[2,3] where the spin structure of the particles is noncollinear, with the spins inclined at an angle to their normal direction due to competing antiferromagnetic exchange interactions at the surfaces of the particles.

Four decades ago Néel anticipated antiferromagnetic nanoparticles (AFNs) to exhibit induced permanent magnetic moments due to the lack of internal structural perfection and/or uncompensated spins on the surface of the particles.[4] Below a critical temperature and particle size, uncompensated spins in AFNs may give rise to a superparamagnetic relaxation of their spin lattices.[1] Moreover, AFNs such as Co_3O_4 have gained increased attention for exhibiting quantum tunneling of magnetization.[5,6] The Co_3O_4 nanoparticle system has also been used in the study of macroscopic magnetic quantum effects and for the production of a mesoporous metal oxide framework structure by nanocasting means employing vinyl-functionalized silica as a template.[7,8] Hence research on synthesis and magnetic studies of Co_3O_4 nanoparticles of desired size and shape has become significant.

Many nanoparticulate metal oxides are prepared by calcination of hydroxide materials.[9] The hydroxides usually decompose at relatively low temperatures (<400 °C), leading to oxide particles with minimal agglomeration and aggregation. Co_3O_4 nanomaterials, too, have been synthesized from cobalt hydroxide and hydroxide materials.[10,11]

Recently we have shown that surfactant intercalated α-hydroxides can be delaminated and colloidally dispersed in alcohols such as 1-butanol.[12] These colloidal dispersions could be used as precursors for oxide nanomaterials with the advantage of running the reaction in organic media, which would allow size control and capping. In this paper, we discuss the synthesis of Co_3O_4 nanoparticles using surfactant intercalated α-cobalt hydroxide, $Co(OH)_{1.67}(DS)_{0.33}\cdot 1.1H_2O$ (DS = dodecyl sulfate), with a structure similar to that of layered double hydroxides[13] as precursor, through a solvothermal hydrolytic decomposition of colloidally dispersed monolayers of the hydroxide material.

Experimental Section

Synthesis. Surfactant intercalated α-cobalt hydroxide was prepared by the addition of 35 mL of a solution containing cobalt acetate and the surfactant (DS) in the mole ratio 1:0.9 into 50 mL of 0.5 M NH_3 solution with constant stirring. The solid product formed was immediately centrifuged, washed free of anions with water followed by acetone, and dried in air at room temperature.

The colloidal dispersion of intercalated α-cobalt hydroxide was prepared by subjecting a mixture of 120 mg of the sample, 25 mg of urea, and 55 mL of 1-butanol to sonication (35 kHz) at room temperature for a half-hour ([Co]/[urea] = 1). The dispersion was then transferred to a Teflon-lined stainless steel autoclave along with 1 mL of water. The sealed autoclave was then placed in an air oven at a temperature of 200 °C for 16 h. The resulting black colloid was centrifuged at 8000 rpm. The solid obtained was washed several times with ethanol and dried to constant weight at 65 °C.

Characterization. All the samples were characterized by chemical analysis, powder X-ray diffraction (Philips X'Pert Pro fitted with a secondary graphite monochromator, Cu Kα radiation, 2° 2θ/min) and infrared spectroscopy (Nicolet Impact 4000 FTIR spectrometer, KBr pellets, 4 cm^{-1} resolution). Transmission electron microscopic (TEM) investigations were carried out using a JEOL 200CX instrument operated at 160 kV. Magnetic data were recorded in the dc mode with a SQUID magnetometer (MPMS R2, Quantum Design) at tem-

* Corresponding authors. (M.R.) Telephone: +91 80 22211429. Fax: +91 80 22245831. E-mail: mikerajamathi@rediffmail.com. (B.H.) Telephone: +49 6421 2825668. Fax: +49 6421 2825653. E-mail: harbrecht@chemie.uni-marburg.de.

[†] St. Joseph's College.

[‡] Indian Institute of Science.

[§] Philipps University.

10.1021/jp050725v CCC: $30.25 © 2005 American Chemical Society
Published on Web 05/24/2005

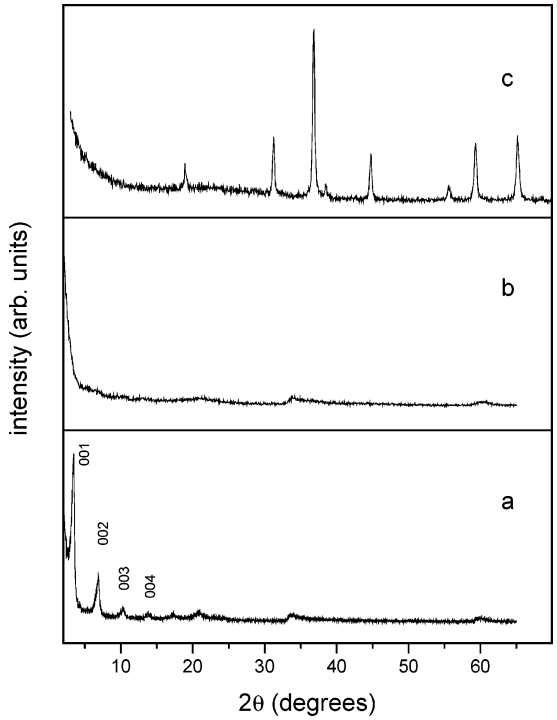

Figure 1. pXRD patterns of (a) as-prepared DS intercalated α-cobalt hydroxide, (b) colloidal dispersion of the α-cobalt hydroxide in butanol, and (c) the product obtained on decomposition of the colloidal dispersion.

peratures ranging from 5 to 350 K at applied magnetic fields up to 2 T. The sample was placed in an ampule manufactured from a KLF (Teflon) tube.

Results and Discussion

The pXRD (XRD = X-ray diffraction) pattern of the as-prepared intercalated α-cobalt hydroxide and the in situ XRD of a dilute colloidal dispersion of α-cobalt hydroxide are shown in Figure 1a,b, respectively. DS intercalated α-cobalt hydroxide (Figure 1a) is reasonably ordered along the layer stacking direction as we observe a series of 00*l* reflections. The basal spacing calculated from these reflections is 25.82 Å. This value confirms the incorporation of the surfactant anions. The alkyl chains of anions are approximately perpendicular to the slabs, and these chains of adjacent layers interpenetrate each other. We also observe the characteristic sawtooth-shaped broad reflections starting at ∼33 and ∼59° due to turbostratic disorder which is common in α-hydroxides.[14] The colloidal dispersion of α-cobalt hydroxide (Figure 1b) shows complete absence of 00*l* reflections, which confirms that the layers have come apart and behave as independent particles.

The pXRD pattern of the solvothermal decomposition product of the α-cobalt hydroxide colloid (Figure 1c) shows all the characteristic peaks of Co_3O_4 and no peaks due to impurities are observed. The particle size, calculated using the Scherrer formula,[15] is ∼35 nm.

Figure 2 shows the IR spectra of DS intercalated α-cobalt hydroxide (Figure 2a) and Co_3O_4 nanoparticles (Figure 2b). In the case of the α-hydroxide (Figure 2a), we observe a broad absorption at 3500 cm^{-1} due to hydrogen bonded hydroxyl groups. C−H stretching vibrations of alkyl chains of the surfactant and S═O stretching vibration of the sulfate group are observed around 2850−2900 cm^{-1} and 1100 cm^{-1}, respectively. In the case of Co_3O_4 nanoparticles (Figure 2b), we observe sharp absorptions of Co(III)−O and Co(II)−O stretching vibrations at 566 and 662 cm^{-1}.[16] Very weak absorptions due to C−H and S═O stretching vibrations indicate that the Co_3O_4 nanoparticles may be very poorly capped by the surfactant.

Figure 3a is a bright field image showing the nanocrystalline nature of the particles. The particles are uniformly 30−35 nm in diameter, matching well with the particle size obtained from pXRD line broadening. However, as seen from Figure 3a (inset, top right) the particles are not spherical but show a characteristic cauliflower-like morphology resulting from the agglomeration of smaller particles each about 3−4 nm in size. Each of these clusters should be a single particle as the pXRD line broadening matches with the size of the cluster rather than the size of the apparent smaller particles. The HRTEM image of the sample (Figure 3c) shows that the particles are crystalline and defect free. The formation of these nonspherical particles confirms that each Co_3O_4 particle has come from one monolayer of the dispersed hydroxide. The collapse of the hydroxide layer during decomposition would lead to a ramified structure as observed here rather than a symmetrical particle. Figure 3b is an SAD pattern from the particles confirming the presence of the Co_3O_4 phase. The rings are broadened considerably, indicating the nanocrystalline nature of the particles.

Figure 4 shows the molar magnetization of coagulated nanoparticulate Co_3O_4 depending on the strength of the magnetic field at selected temperatures between 5 and 350 K. A small hysteresis loop is observed at any temperature. The coercive force amounts to 42(7) G and is fairly constant within the temperature range 5−350 K. The remanence increases slightly with decreasing temperature; compare inset Figure 4. The saturation magnetization M_s was determined from the extrapolation of a linear fit of M versus H at fields above 1 kG to zero field. As seen from the upper graph of Figure 5, a plot of M_s versus temperature shows a steep increase of M_s below 20 K indicative of a weak ferromagnetic transition. The transition occurs a few degrees below the blocking temperature of superparamagnetic, nanoparticulate Co_3O_4 displayed by a maximum in the magnetization for a zero field cooled sample.[8,10] We associate the transition with an intrinsic property of the nanogranular sample since a thermoremanent magnetization experiment (TRM)[17] revealed a comparable evolution of magnetization with temperature. The discontinuous change was found at about 12 K below the Néel temperature T_N of bulk crystalline Co_3O_4;[18,19] see Figures 5 and 6. In this experiment, the sample was slowly cooled from 350 to 5 K in an applied magnetic field of 5 kG. Hereafter, the field was switched off to record the disappearance of the remnant magnetization while the sample was slowly heated to 350 K.

Further specific properties of nanoparticulate Co_3O_4 become apparent from a plot of the inverse molar susceptibility χ_{mol} versus temperature. The plot recorded at 5 kG is depicted in Figure 6. The data were corrected for diamagnetic contributions of the sample holder and the sample (-8×10^{-5} emu/mol[19]) and for the saturation magnetization. A fit of the plot to a Curie−Weiss equation ($R^2 = 0.9995$) yields an effective magnetic moment of 5.05(4) μ_B and a Weiss temperature $\theta = -118.8(5)$ K. These quantities contrast with those of bulk crystalline Co_3O_4, 4.14 μ_B and $\theta = -53$ K.[19] A moment of 3.02 μ_B was determined for Co^{2+} in the antiferromagnetic state (<40 K) by means of neutron diffraction.[20] Associated with the increase of the effective moment in the nanogranular sample compared to the value of bulk Co_3O_4 is the onset of a ferromagnetic ordering below 30 K displayed by a sudden decline of the inverse magnetic susceptibility, χ^{-1}. The change

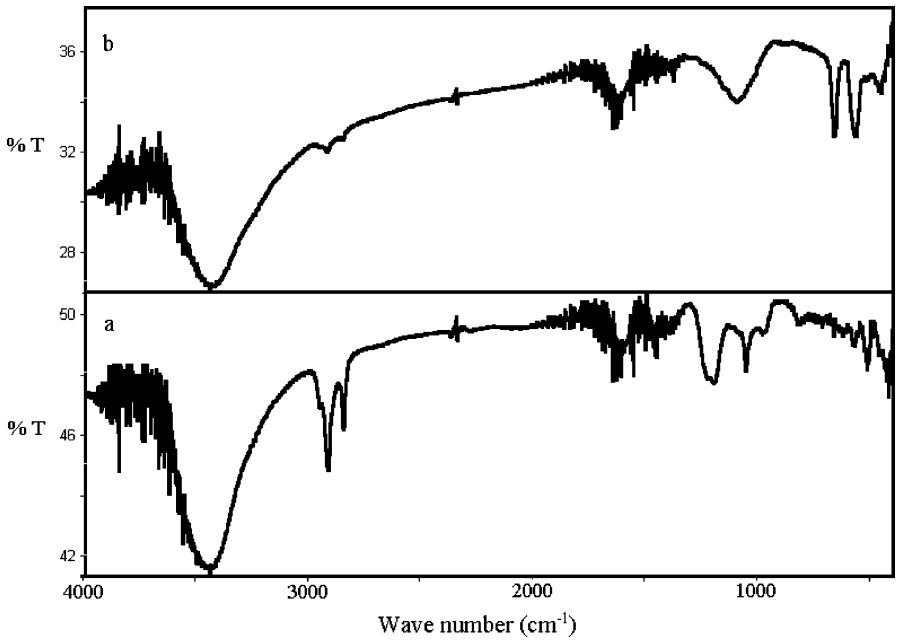

Figure 2. IR spectra of (a) DS intercalated α-cobalt hydroxide and (b) the product obtained on decomposition of the colloidal dispersion of the α-hydroxide.

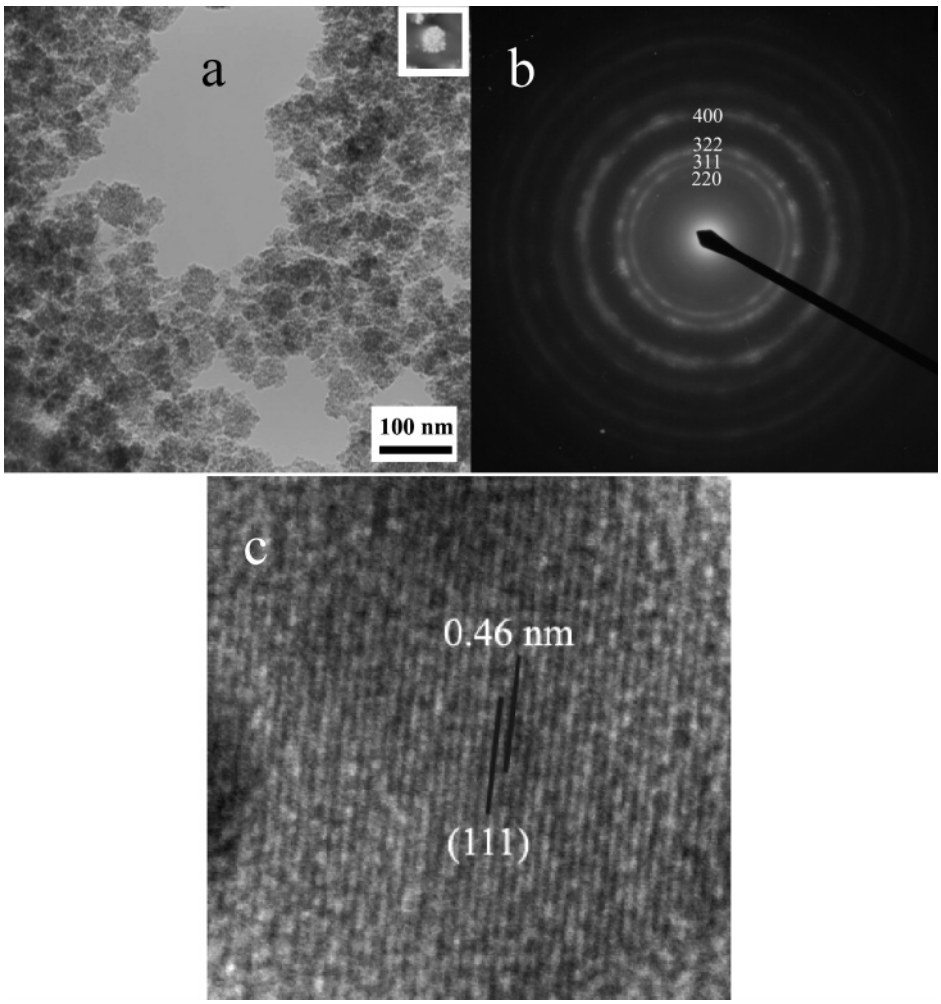

Figure 3. (a) Bright field image showing very small particles forming a cluster to give a cauliflower morphology. Inset shows the dark field image where the smaller particles can be seen clearly (the scale bar for the inset is same as that of the main figure). (b) SAD pattern from the particles. (c) HRTEM image of a region of the sample showing lattice fringes from the 111 planes.

from an antiferromagnitic state for bulk Co_3O_4 to a weakly ferromagnetic state for nanoparticulate Co_3O_4 can be rationalized by supposing that a noticeable part of Co^{3+} (d^6 low spin) and Co^{2+} (d^7) ions switched octahedral and tetrahedral sites,

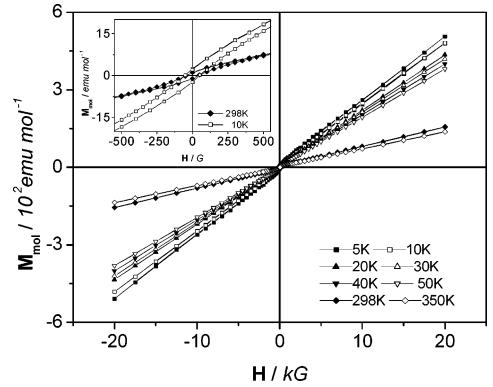

Figure 4. Magnetization curves as a function of applied magnetic field of nanoparticulate Co_3O_4 at various temperatures. The inset in the upper left shows a magnification of the hysteresis loops at 10 and 298 K.

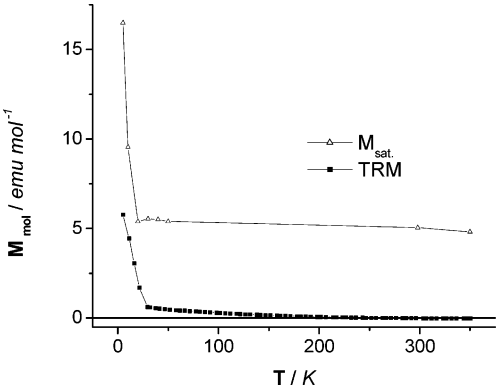

Figure 5. Saturation magnetization versus temperature for nanoparticulate Co_3O_4 compared to TMR data recorded after cooling at 5 kG.

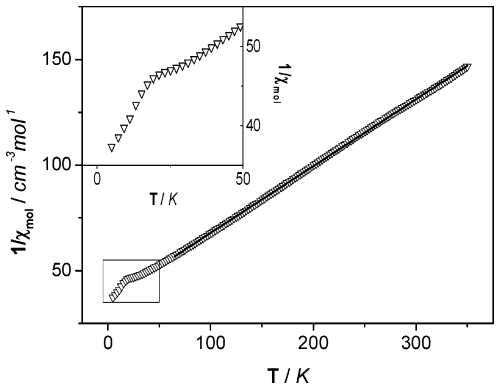

Figure 6. Reciprocal susceptibility versus temperature of nanoparticulate Co_3O_4 measured in an applied field of 5 kG. The line reproduces the linear fit of the data to a Curie−Weiss equation, $\chi = C/(T - \theta)$.

probably by local electron hopping. As a consequence of such a partly inverted spinel structure, the antiferromagnetic interactions between Co ions on the tetrahedral sites do not annihilate. Moreover, cooperative magnetic interactions between Co^{2+} on octahedral sites and $Co^{2+/3+}$ on tetrahedral sites below T_N can amplify the ferrimagnetic interactions. On the other hand, cooperative interactions between uncompensated spins on the surface may also give rise to weakly ferromagnetic properties. In view of the relatively large size of the particles (∼35 nm), however, intra- or interparticular interactions of uncompensated spins at the surface seem to be unlikely to dominate the conversion from an antiferromagnetic to ferromagnetic state at low temperature. Note the increase of the effective moment is

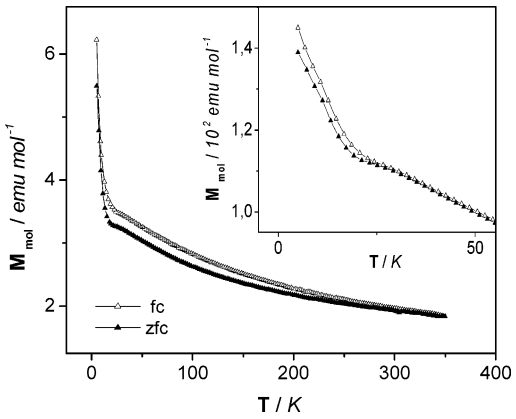

Figure 7. zfc and fc magnetizations versus temperature at applied magnetic fields of 50 G and 5 kG (insert) of nanoparticulate Co_3O_4.

about 25%. A guestimate based on the measured effective moment of 5.05 μ_B and neglecting spin−orbit coupling and uncertainties with respect to the spin states of the interchanged Co^{3+} and Co^{2+} ions amounts to a degree of inversion of about 7%. Thus, we assume that volume effects contribute decisively to the ferromagnetism of nanogranular Co_3O_4.

Magnetic interactions in and between Co_3O_4 nanoparticles were studied by recording magnetization data in the so-called zero-field-cooled (zfc) and field-cooled (fc) mode.[21] To this end, the magnetization was measured in the presence of a given magnetic field upon heating after cooling the sample to low temperature in the absence of an external field. Hereafter, data were recorded in an applied field of the same strength upon cooling and heating. Two pairs of cycles are shown in Figure 7, one measured at 50 G and a second at 5 kG. The relevant part of the second pair is shown in the inset. Remarkably, no cusp appears in the zfc magnetization curve, indicating a blocked superparamagnetic state usually observed for dispersed paramagnetic nanoparticles upon heating. Superparamagnetism, as before ascertained for Co_3O_4 nanoparticles,[8,10] seems to be suppressed in the agglomerated sample due to the fairly strong interactions between the particles in the cauliflower-like crops; see Figure 3a. Nevertheless, the corresponding pairs of zfc and fc magnetization curves exhibit three noteworthy features reflecting the nanoparticulate character of the sample:

(i) In all cases where the zfc and fc magnetizations diverge, the zfc value is smaller than the fc value, reflecting the tendency of the particles to minimize the magnetocrystalline energy under zfc conditions.

(ii) At an applied field of 50 G, the two curves bifurcate upon cooling already at about 320 K. Apparently the magnetic field is too small to overcome the activation energy for a minimization of the Zeeman energy, even at elevated temperatures. Concomitantly the effective moment derived from a $1/\chi$ versus T plot recorded at 500 G in the zfc mode is reduced to 5.20(8) μ_B compared to the value of 5.47(9) μ_B for the corresponding fc measurement.

(iii) At an applied field of 5 kG the magnetizations recorded in the zfc and fc mode bifurcate upon cooling at the onset of ferrimagnetic ordering. Thus, a magnetic field of 5 kG enables an optimization of the Zeeman interactions in the paramagnetic state.

Conclusions

The hydrolytic solvothermal decomposition of a colloidal dispersion of dodecyl sulfate intercalated α-cobalt hydroxide yields nanoparticulate Co_3O_4 with a cauliflower-like morphology

resulting from the fusion of 3−4 nm particles into grains, each about 35 nm across. The grains are weakly ferromagnetic. A reinforcement of the effective magnetic moment of about 25% is found compared to the moment of tetrahedrally coordinated Co(+II) in bulk Co_3O_4. Ferrimagnetic ordering below 28 K and the amplified magnetic moment can be rationalized assuming that nanogranular Co_3O_4 has a partly inverted spinel structure.

Acknowledgment. This work was partially funded by DST, New Delhi, and by the Stock of the German Chemical Industry, FCI. M.R. thanks SSCU, Indian Institute of Science, Bangalore, for providing pXRD facilities and Royal Society of Chemistry, London, for a Journal Grant for Authors.

References and Notes

(1) Chikazumi, S. *Physics of Ferromagnetism*; Oxford University Press: New York, 1997.

(2) Martinez, B.; Obradors, X.; Balcells, L.; Rouanet, A.; Monty, C. *Phys. Rev. Lett.* **1998**, *80*, 181.

(3) Kodama, R. H.; Berkowitz, A. E.; McNiff, E. J., Jr.; Foner, S. *Mater. Sci. Forum* **1997**, *643*, 235.

(4) Néel, L. In *Low-Temperature Physics*; Dewitt, C., Dreyfus, B., de Gennes, P. D., Eds.; Gordon and Breach: New York, 1962; p 413.

(5) O'Caldera, A.; Legget, A. J. *Phys. Rev. Lett*. **1981**, *46*, 211.

(6) Chudnovsky, E. M. *J. Appl. Phys.* **1993**, *73*, 6697.

(7) Takada, S.; Fujii, M.; Kohiki, S.; Babasaki, T.; Deguchi, H.; Mitome, M.; Oku M. *Nano Lett.* **2001**, *1*, 379.

(8) Wang, Y.; Yang, C.-M.; Schmidt, W.; Spliethoff, B.; Bill, E.; Schueth, F. *Adv. Mater.* **2005**, *17*, 53.

(9) Cushing, B. L.; Kolesnichenko, V. L.; O'Connor, C. J. *Chem. Rev.* **2004**, *104*, 3893.

(10) Makhlouf, S. A. *J. Magn. Magn. Mater*. **2002**, *246*, 184.

(11) Xu, R.; Zeng, H. C. *J. Phys. Chem. B* **2003**, *107*, 926.

(12) Nethravathi, C.; Harichandran, M.; Shivakumara, C.; Ravishankar, N.; Rajamathi, M. *J. Colloid Interface Sci.*, in press.

(13) Kamath, P. V.; Therese, G. H. A.; Gopalakrishnan, J. *J. Solid State Chem.* **1997**, *128*, 38.

(14) Rajamathi, M.; Kamath, P. V.; Seshadri, R. *Mater. Res. Bull*. **2000**, *35*, 271.

(15) Scherrer, P. *Göttinger Nachrichten* **1918**. Patterson, A. L. *Phys. Rev.* **1939**, *56*, 978.

(16) Li, S.; Bi, H.; Cui, B.; Zhang, F.; Du, Y.; Jiang, X.; Yang, C.; Yu, Q.; Zhu, Y. *J. Appl. Phys.* **2004**, *95*, 7420.

(17) Panissod, P.; Malinowska, M.; Jedryka, E.; Wojcik, M.; Nadolski, S.; Knobel, M.; Schmidt, J. E. *Phys. Rev. B* **2001**, *63*, 014408.

(18) Cossee, P. *J. Inorg. Nucl. Chem*. **1958**, *8*, 483.

(19) Roth, W. L. *J. Phys. Chem. Solids* **1964**, *25*, 1.

(20) Landolt-Börnstein. *Neue Serie*; Springer-Verlag: Berlin, 1979; Band II/2.

(21) Hansen, M. F.; Mørup, S. *J. Magn. Magn. Mater*. **1999**, *203*, 214.